Electrochemically Triggered Selective Adsorption of Biotemplated Nanoparticles on Self-Assembled Organometallic Diblock Copolymer Thin Films

*Jean-Charles Eloi, Sarah E. Ward Jones, Veronika Poór, Mitsuhiro Okuda, Jessica Gwyther, and Walther Schwarzacher**

The controlled adsorption of the iron-containing cage protein ferritin at the nanoscale using stimuli-responsive self-assembled diblock copolymer thin-film templates is reported. The diblock copolymer used study consists of a cylinder-forming polystyrene-*block*-polyferrocenylsilane (PS-*b*-PFS), with PFS as the minor block, and shows reversible redox properties. To prevent any spontaneous protein adsorption on either block, the electrolyte pH is selected to leave the ferritin negatively charged, and the protein concentration and solution ionic strength are carefully tuned. Selective adsorption of ferritin on the PFS domains of the self-assembled thin films is then triggered in situ by applying a positive potential, simultaneously oxidizing the PFS and attracting the ferritin electrostatically.

1. Introduction

The organization of bioactive proteins into arrays of functional molecules has attracted much interest because of potential applications in the growing field of bionanotechnology such as biomolecular electronics, biosensors and miniaturized assays for low-volume biological tests.[1] Patterns of proteins bearing functional nanoparticles[2] have also attracted much interest especially for the fabrication of quantum dot arrays[3] and for the growth of carbon nanotubes at precise locations.[4]

To date, the arrangement of proteins has been mainly accomplished using microscale patterning by a wide variety of methods such as microcontact imprinting, lithography, high-precision contact-printing robotics, or ink-jet printing.[5] These methods are top-down techniques that can require complex and expensive equipment and they typically yield protein patterns on a length scale where a sub-100-nm arrangement is a challenge.[6] To achieve patterning down to the length scale of individual proteins (~10 nm), methods including colloidal self-assembly,[7] anodic porous alumina[8] and block copolymer self-assembly[9] have been introduced. Although these are bottom-up methods, most of them include extra fabrication steps, such as lithography, metal evaporation or other chemical post-treatment before they can be applied to protein adsorption. A few groups have nevertheless used commercially available polystyrene-*block*-poly(methylmethacrylate) (PS-*b*-PMMA) to create nanoarrays of hydrophobic PS on which proteins adsorb selectively[10] but their studies lacked external control over the trigger of adsorption.[11]

Diblock copolymers contain two chemically distinct polymer segments (blocks) that are covalently bridged and tend to phase separate in the solid phase into nanodomains, the size of which is governed by the chain lengths of the blocks. By controlling the blocks' volume fraction, morphologies such as spheres, cylinders and lamellae can be achieved.[12] In cast thin films the boundary conditions, such as the substrate chemistry and film thickness, can orient periodic arrays of cylinders perpendicularly to the substrate.[13]

Polyferrocenylsilanes (PFS), belong to a well-studied class of organometallic polymers that contains alternating iron centres and organosilicon in the main chain.[14] PFS, and PFS-containing diblock copolymer thin films, exhibit redox-active properties in solution[15,16] and in the bulk[17,18] associated with the reversible Fe^{II}/Fe^{III} couple.[19]

Among biomolecules, cage-like proteins and viruses are of particular interest in nanotechnology as they can act as active templates for the size- and shape-controlled synthesis of monodisperse nanoparticles.[20] Widely used in research,[21] ferritin is an iron storage protein found in most mammals and plants. 24 subunits form a spherical cage (monomer) of fixed external diameter (12 nm) enclosing a central cavity of approximately 8 nm in diameter. In nature, ferritin regulates the iron content in organisms by a complex ion exchange process through its ion channels. In the laboratory, ferritin can crystallize a wide variety of minerals in its central cavity, including transition metal oxides,[22] quantum dots,[23] catalysts[24] and iron and cobalt magnetic oxides.[25] The protein shell has other convenient uses as it can direct the 2D and 3D self-assembly of the synthesized nanoparticles by protein crystallisation[26] or layer-by-layer

Dr. J.-C. Eloi, Dr. S. E. Ward Jones, V. Poór,
Dr. M. Okuda, Prof. W. Schwarzacher
H. H. Wills Physics Laboratory
University of Bristol
Bristol, BS8 1TL, UK
E-mail: w.schwarzacher@bristol.ac.uk
Dr. J. Gwyther
School of Chemistry
University of Bristol
Bristol, BS8 1TS, UK

DOI: 10.1002/adfm.201200210

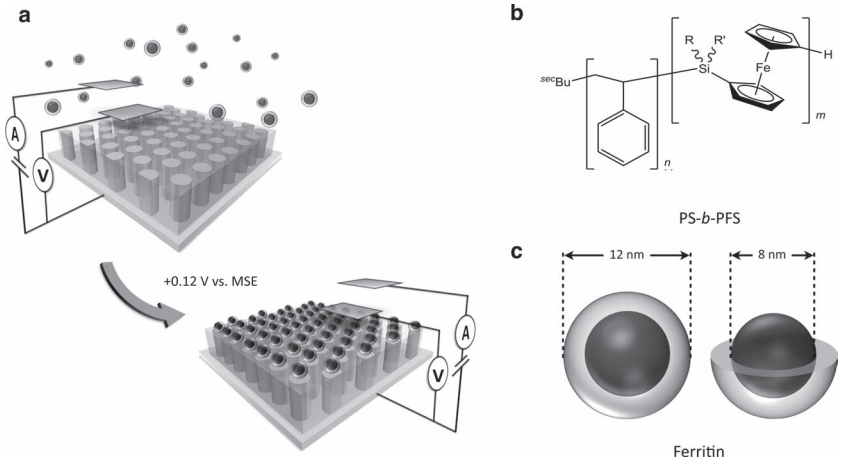

Figure 1. a) schematic representation of the *in situ* potential-triggered, selective adsorption of ferritin molecules onto a self-assembled diblock copolymer thin film; b) structure of PS-*b*-PFS diblock copolymer used in this study, with R and R′ = $(CH_2)_n$-CH_3, n = 0 and 1; and c) schematic of a ferritin molecule with the peptide shell (12 nm diameter) around the iron containing core (8 nm diameter).

assembly.[27] The subunit assembly also provides, independently of the nature of the nanoparticle, a pH-dependent surface charge distribution, thus allowing precise control over adsorption at charged surfaces.

In this article, we apply PS-*b*-PFS thin films as redox-active nanopatterned surfaces that not only direct where ferritin adsorption takes place but also allow the trigger of this event. This new approach permits on/off control over the selective adsorption of ferritin at the nanoscale (**Figure 1**) and would allow, for instance, the fabrication of nanopatterned arrays of discreet functional biotemplated nanoparticles.

2. Results and Discussion

2.1. Protein Adsorption Conditions

To achieve potential-triggered adsorption of ferritin on PS-*b*-PFS thin films, it is necessary to create an environment where no or very few proteins adsorb via hydrophobic interactions on either the PS or PFS domains, but where a slight change in charge on the PFS domains favours preferential ferritin adsorption.[28] For this, careful tuning of the solution ionic strength, pH and ferritin concentration are required.

The isoelectric point of ferritin is in the range of pH 4.5–4.8. This means that ferritin has a negative net charge above this pH and a positive one below. We worked above pH 5 so that ferritin would be attracted to oxidized PFS which is positively charged. The buffer concentration also has a strong effect on protein adsorption at surfaces. At higher ionic strengths, i.e. shorter Debye lengths,[6a] ferritin adsorbed readily on the PS-*b*-PFS thin film to form a monolayer or aggregates even before the PFS was oxidized. However, this effect decreased with decreasing salt concentration, as ferritin molecules were repelled from the surface due to the repulsive electrostatic fields extending further into the solution from the surface. As a result, all subsequent protein adsorption studies were conducted in low ionic strength 50 mM sodium perchlorate ($NaClO_4$), pH 6, with very low protein concentrations, typically around 5 μg mL^{-1}, to avoid protein aggregation on a short timescale (see supporting information regarding these studies).

2.2. Redox Activity

The electrochemical behavior of a spin-coated thin film of thiol-terminated PFS (PFS-SH) was studied with an electrochemical quartz crystal microbalance (E-QCM) to find the best potential window for adsorption studies (polymer and adsorption data in **Table 1**). **Figure 2** shows E-QCM and CV plots for a PFS-SH thin film in $NaClO_4$ solution (50 mM, pH 6.2 at room temperature) measured between –0.3 and +0.3 V at a scan rate of 10 mV s^{-1}. All potentials are quoted relative to the saturated mercury sulfate reference electrode (MSE). The data show a two-wave oxidation and reduction, and this behavior is highly reproducible. The first and second oxidation waves have peaks at +0.09 V and +0.13 V vs. MSE, respectively. This two-wave oxidation response was previously demonstrated for PFS oligomers in solution, where the first oxidation wave was attributed to the oxidation of every other iron center and the second wave, at higher energy, to the remaining sites.[15] In the

Table 1. Compositional and E-QCM data for the polymers studied.

polymer	PFS volume fraction, ΦPFS	Mn [kg mol^{-1}]	DPn[a)]	PDI[b)]	Charge, Q [μC]	Δf [Hz]
PS	0	46	440	1.05	17.8	–0.5
PFS-SH	1	478	1490	1.15	204.2	–11.1
PS-*b*-PFS	0.23	79	553 (PS), 83 (PFS)	1.05	76.6	–3.7

[a)] Degree of polymerization; [b)] Polydispersity index.

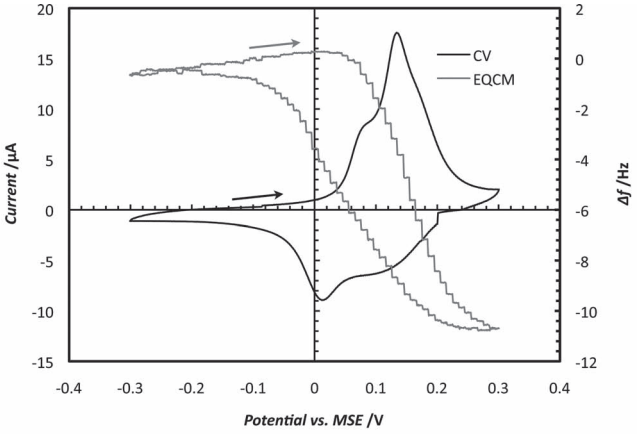

Figure 2. E-QCM and CV data for a thin film of PFS-SH at room temperature in 50 mM $NaClO_4$. The scan rate is 10 mV s^{-1}. The reference and counter electrodes are saturated mercury sulfate and platinum, respectively.

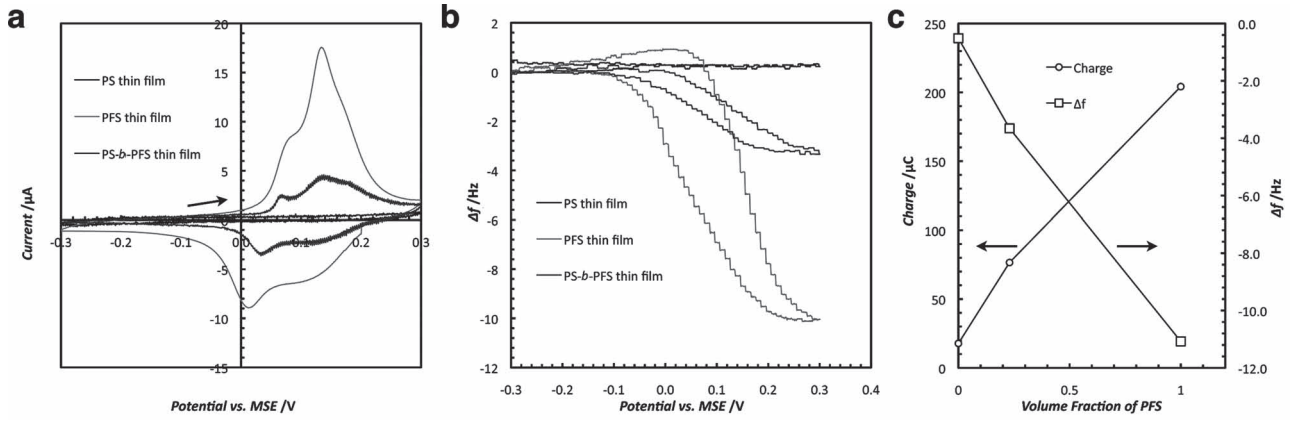

Figure 3. CV (a) and E-QCM (b) plots for thin films of PS (black lines), PS-*b*-PFS (dark grey lines), and PFS-SH (light grey lines, repeated from Figure 2 for comparison) at room temperature in $NaClO_4$ 50 mM. The CV scan rate is 10 mV s^{-1}. The reference and counter electrodes are saturated mercury sulfate and platinum, respectively. c) Charge associated with the oxidation wave and corresponding E-QCM frequency drop for PS and PFS-SH homopolymers and PS-*b*-PFS diblock copolymer thin films of similar thicknesses. The electrode area was the same in each case.

case of polymers, the two waves are merged together and sometimes not discernible due to chain length polydispersity.

Upon oxidation, the PFS-SH thin film became charged and more hydrophilic. The E-QCM permits us to observe the change in mass associated with the adsorption of counterions during this redox cycle. From Figure 2, the QCM frequency drops at the onset of the first oxidation wave at around +0.05 V vs. MSE and this drop continues uninterrupted until the end of the second oxidation wave. Upon reduction, the frequency returned to its original value. This reversible process was attributed to the adsorption/desorption of perchlorate (ClO_4^-) ions from the electrolyte to balance the additional positive charge on the Fe ions.[29] From the Sauerbrey equation (Equation 1), the observed frequency drop, $\Delta f = -11 \pm 0.1$ Hz (Table 1), and the global charge under the two-wave oxidation curve ($Q = 204 \pm 10$ µC) can be used to calculate the molar mass $M_{moieties}$ of the adsorbed moieties, Equation 2. Assuming $z_{moieties} = 1$ (charge of the perchlorate ion), we find $M_{moieties} = 94 \pm 5.5$ g mol^{-1}, which is in agreement, within error, with the perchlorate ion molecular weight ($M_{ClO_4^-} = 99.5$ g mol^{-1}).

When cast the same way, PS-*b*-PFS diblock copolymer films showed a self-assembled morphology consisting of mainly upright, but also lying down, PFS-rich cylindrical domains surrounded by a PS matrix.[30] Typical dimensions from AFM analysis gave a cylinder periodicity of 39 nm and a cylinder diameter of 20 nm (these results were in agreement with the overall volume fraction of the polymer). Both PS and PFS are expected to wet the gold surface as a result of similar water contact angles (90 and 94 ± 1°, respectively).[30,31] This results in non-selective wetting of the conductive substrate by each block, allowing both blocks to be present at the substrate/film interface and also at the film/air interface for films with thicknesses incommensurate with the diblock copolymer periodicity.[13] In our case, the film thicknesses are below 30 nm and the PFS cylinders are expected to form a continuous connection from the gold electrode through to the film surface, later in contact with the electrolyte and the ferritin, for an upright-cylinder morphology.

Nevertheless, previous studies using conductive AFM measurements confirmed that the electro-active PFS blocks make a charge bridge between the surface of the film and the gold substrate for lying-down cylinders.[18] On a mixed morphology PS-*b*-PFS thin film, electrochemical measurements showed a double-wave oxidation on CV scans (**Figure 3**a, dark grey curve), typical of the PFS redox response, indicating a charge bridge between the electrode and the electrolyte. A PS thin film undergoing the same scans did not show any peak, proving inert over this potential range (Figure 3a, black curve). The reversible adsorption and desorption of perchlorate ions was also observed for the PS-*b*-PFS thin films (Figure 3b, dark grey curve) and the value of the frequency change, Δf (see Table 1), corresponded to the amount of PFS present in the diblock (volume fraction $\Phi_{PFS} = 0.23$). Integration of the oxidation waves showed that the total charge is also proportional to the volume fraction of PFS (Figure 3c) compared with PS and PFS-SH thin films of similar thicknesses (data in Table 1). This not only confirmed the electroactive bridging between electrode and surface but also confirmed that most of the PFS domains were involved.

2.3. Potential-Triggered Protein Adsorption

Ferritin adsorption was monitored by E-QCM. At the start of each experiment, the polymer-coated electrode was placed in the $NaClO_4$ electrolyte without a potential applied. The potential was then set to –0.2 V, in the region where PS, PFS and PS-*b*-PFS show no electrochemical signal. After stabilization of the QCM frequency, the potential was stepped to +0.2 V and the experiment left to stabilize. After a further 10 min, ferritin (in 50 mM $NaClO_4$, pH 6.2) was added (the final ferritin concentration was 6.5 µg mL^{-1}).

For PS, there was little protein adsorption at either +0.2 or –0.2 V (**Figure 4**a, light grey solid line) and no adsorption of perchlorate ions upon initially switching the potential from –0.2 to +0.2 V. Although the slow drift of frequency over time indicated some ferritin adsorption, this was minimized, on the timescale of the experiment, by the combination of a pH above the ferritin isoelectric point and the low ionic strength. The

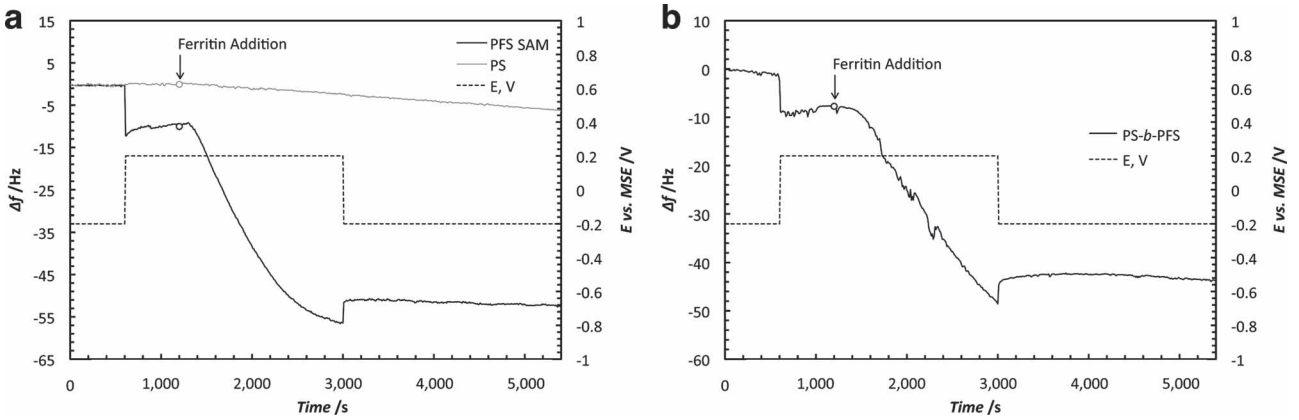

Figure 4. E-QCM plots of the adsorption of ferritin (addition 10 minutes after potential change, represented by -○-) on PS homopolymer thin film (a, solid light grey line), PFS-SH self-assembled monolayer (SAM) (a, solid black line) and PS-*b*-PFS diblock copolymer thin film (b, solid black line). The experiments were made at room temperature in 50 mM $NaClO_4$ at the applied potential indicated by the dotted line.

negative charge on ferritin and high Debye length minimizes the likelihood of a ferritin molecule approaching the surface sufficiently close for hydrophobic interactions to induce adsorption.

For a PFS-SH self-assembled monolayer (SAM), the change in potential from –0.2 to +0.2 V induced the adsorption of ClO_4^- ions, indicating an electrochemically active surface (Figure 4a, black solid line). The process was instantaneous and step-like, showing rapid saturation of all ferrocene sites on the polymer (the polymer is almost fully oxidized at this potential, Figure 2). When ferritin was then added, the QCM frequency started to drop significantly, following a typical protein-adsorption trend.[32] The process was stopped at t = 3000 s when the potential was reset to –0.2 V, where PFS is neutral again. This did not release all the previously adsorbed moieties but only a few, presumably mainly the remaining ClO_4^- ions that were not displaced by ferritin molecules. This suggests that most ferritin molecules were trapped in the "bulk" of the SAM. The change from a charged and hydrophilic to neutral and hydrophobic polymer is very fast compared to the adsorption of proteins. When the potential is set to +0.2 V, PFS uncoils and extends into the electrolyte. Vancso *et al.* observed a volume change attributed to a change in solubility, electrostatic interactions between the charged ferrocene centres and flexibility due to the stretching of the chains.[33] When the potential is reset to –0.2 V, the PFS chains become almost instantaneously uncharged and coil back into a compact thin film, trapping ferritin molecules at the same time. No adsorption was observed after t = 3000 s, consistent with the absence of ferritin adsorption under these conditions on an uncharged PFS surface. This was confirmed by repeating the experiment on a PFS-SH SAM sample maintained at E = –0.2 V before and after the ferritin addition (see supporting information).

The same technique was then applied to a self-assembled PS-*b*-PFS modified QCM electrode. Figure 4b shows the adsorption of ferritin 10 minutes after switching to +0.2 V. The similarity between the two adsorption curves in Figure 4a,b indicates that the adsorption process is mainly dominated by the PFS block. To further confirm this, the data in Figure 4a,b were normalized to the PFS content. To achieve this, we assumed that the decrease in frequency where only ClO_4^- ions adsorbed was directly proportional to the PFS content involved in the process, as no adsorption was observed for PS alone. By normalizing the two curves in this way, the ferritin adsorption slope followed a similar gradient and reached the same final plateau when the potential was returned to –0.2 V (see supporting information). This suggested that whether PS is present or not, ferritin adsorption only happened at the PFS block and that most of the PFS block (whether the domains are upright or lying down) took part in the adsorption process.

AFM images were recorded to confirm selective ferritin adsorption on the PFS domains, after holding the potential at E = +0.12 V, where around half of the chains' ferrocene centres are oxidized (Figure 3a, dark grey line) for 250 seconds, the time needed to give a change in frequency Δf of a few hertz. This potential should prevent chains from uncoiling too much in the electrolyte, preventing proteins from being trapped in the bulk upon reduction while still providing sufficient charge to interact with ferritin. Although our imaging method involved further preparation steps after adsorption (the rinsing of the sample with water and the drying with N_2) and might not necessarily reflect *in situ* aqueous adsorptions, the distribution of ferritin molecules was seen to follow the PFS nanodomains pattern. **Figure 5** shows the phase image of a lying-down-cylinder area on a PS-*b*-PFS thin film sample where ferritin was adsorbed at +0.12 V for 250 s before being rinsed, dried and imaged. The phase contrast allows us to distinguish between PS, PFS and especially ferritin, as isolated whiter spots that are observed only on one of the blocks. These spots appear to be positioned exclusively on the PFS domains as attested by comparison with the AFM height profile (see Supporting Information). A height analysis confirmed the presence of single ferritin molecules aligned on the redox-responsive PFS cylindrical domains, confirming the E-QCM study. Nevertheless the proteins are not forming a continuous wire presumably due to interparticle electrostatic repulsion.

3. Conclusions

In summary, we have developed a facile, bottom-up technique to create nanopatterned arrays of ferritin molecules by

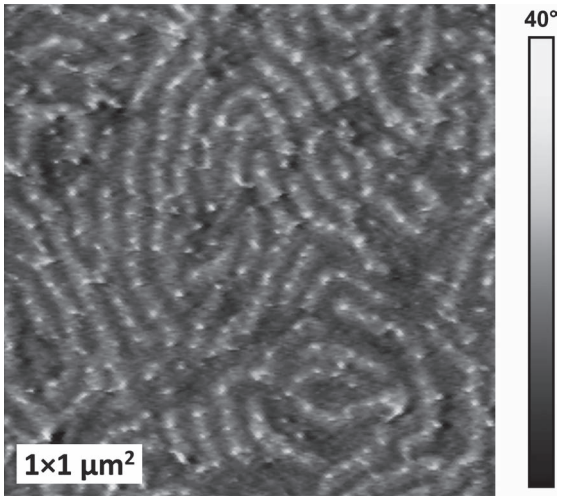

Figure 5. AFM phase image of a PS-*b*-PFS thin film area with lying-down cylinders bearing ferritin molecules (whiter dots). The adsorption was done at E = +0.12 V vs. MSE for 250 s.

externally-triggered adsorption using self-assembled PS-*b*-PFS thin films. Self-assembly of PS-*b*-PFS thin films gave a cylindrical morphology with stable, redox-active PFS domains that acted as charge bridges between the gold layer and the electrolyte whether the cylinders were lying down or in an upright morphology. Ferritin adsorption was initiated *in situ* on the electroactive PFS sites when a positive bias (typically + 0.12 V vs. MSE) was applied.

Our simple bottom-up approach using redox-responsive PS-*b*-PFS could be extended to larger surface areas as research is being actively conducted on fabricating long-range ordered diblock copolymer thin films.[34] AFM nanoxerography[35] could also be used to charge domains selectively and thereby create more intricate patterns of adsorbed proteins. We believe our work could be extended to other types of ferritin molecules carrying synthetic nanoparticles, generating additional functionality. For example, magnetoferritin arrays are currently of interest for magnonics applications where spin waves, like light for photonics, are used to carry and process information.[36]

4. Experimental Section

Materials and Equipment: Polystyrene (PS) and polystyrene-*block*-polyferrocenylsilane (PS-*b*-PFS) were synthesized by living anionic polymerization according to previously reported methods.[37] Thiol-terminated polyferrocenylsilane (PFS-SH) was prepared by a slight modification of the standard living anionic polymerization of [1] silaferrocenophanes, end-capping the living PFS chains with a slight excess of propylene sulfide.[38] This resulted in PFS-$(CH_2)_n$-SH, with short alkane chains (low n values), interfering only slightly with the charge transport upon oxidation. Horse spleen ferritin (Fluka, Switzerland) was purified through a Sephacryl S-300 HR gel chromatography column (GE Healthcare, UK). The monomeric fractions (here, a monomer refers to one ferritin molecule) were isolated and native polyacrylamide gel electrophoresis (PAGE) of an aliquot confirmed the absence of dimers and trimers. Purification used MilliQ water (18.2 MΩ cm) with Tris-HCl (50 mM, pH 8.15) in which the ferritin monomers were also stored at +4 °C. When necessary, the buffer was exchanged via sequential centrifugation steps, using Centriprep YM 50 (Millipore, Ireland) in an Avanti J-E Centrifuge System (Beckman Coulter, CA, USA), replacing the filtrate each time by fresh $NaClO_4$ electrolyte (50 mM, pH 6). Typically, after 5 × 10 mL filtrations, the buffer was exchanged. The concentrations of the ferritin solutions were determined by the Bradford method.[39] A clean room, class 1000 (ISO 6) was used for the spin coating of polymers, as well as for sample preparation and study of the adsorption conditions. The cleanroom was also used for substrate handling, AFM sample preparation and storage of all samples.

Thin Film Preparation: Polymer thin films were prepared by spin-coating from a toluene solution (3.0 mg mL^{-1}) with a Spin 150 (SPS, the Netherlands). A two-step program was used involving a short, low-speed part followed by the spinning itself at much higher rotation speed (10 s at 500 rpm followed by 90 s at 5000 rpm with a 500 rpm s^{-1} acceleration). The first step helped spread the solution evenly on the substrate while the second provided a quick solvent evaporation, normal to the surface. Typically, the PS and PFS-SH thin film thicknesses were in the range of 20 to 30 nm. The substrates used for the study were Si wafers with native oxide, when no electrochemistry was needed, and evaporated gold on quartz for E-QCM measurements. All solutions were filtered through a PTFE membrane filter (0.22 μm) before spin coating. Solvent annealing was carried out at room temperature in the absence of moisture under a flow of argon bubbled through toluene. In this study, we used PFS-SH SAMs and PFS-SH thin films. Upon oxidation, PFS becomes more hydrophilic, hence more soluble in aqueous media. It was therefore important to anchor the chains to the substrate for long experiments such as adsorption studies where SAMs were used. However on the timescale of cyclic voltammetry (CV), cast PFS-SH thin films were used for better comparison with the diblock copolymer ones. These films remained undamaged, as attested by the reproducible CVs, although not all chains are tethered to the gold substrate.

Protein Adsorption Screen Tests: Protein adsorption screening studies were performed in a cleanroom on PS, PFS and PS-*b*-PFS coated Si wafers. The wafers were cut to convenient squares (~5 mm) after spin-coating of the polymer. Each square was put in one well of a 48-well assay plate and a drop of the solution (25 μL, ferritin in buffer) was placed on the substrate for typically 30 min. After this, the buffer solution (300 μL, no ferritin) was put in each well to break the drop and dilute the protein solution. Subsequent washings with MilliQ water (5 times) were performed to wash away the buffer and the ferritin remaining in solution before the square samples were taken out of each well and dried with a light flow of N_2.

E-QCM: A QCM200 Quartz Crystal Microbalance Digital Controller (SRS, CA, USA) was used with a QCM25 Crystal Oscillator. 1-inch Crystals (SRS, CA, USA) with Au evaporated on Cr, AT-cut, with a resonant frequency of 5 MHz (exposed gold area of 1.37 cm^2) were used and cleaned with nitric acid prior to spin-coating.[40] The Kynar (Polyvinylidene fluoride) sample holder was bought from SRS. The apparatus was used with an Autolab potentiostat (see next paragraph). Measurements were made at laboratory room temperature after frequency stabilization for several minutes. During this stage, the circuit's capacitance was nulled. The QCM gate was set at 1 s with a 200 Hz scaling factor. Measurements were started when the noise in the measured frequency was less than 0.1 Hz. The QCM records frequency shifts of the crystal resonator. These changes are related to the mass adsorbed on the electrodes by the Sauerbrey equation:[41]

$$\Delta f = -C_f \times \Delta m \tag{1}$$

with

$$\Delta m_{\text{moieties}} = \Delta Q \times M_{\text{moieties}} / (z_{\text{moieties}} \times F) \tag{2}$$

where Δf and Δm are the frequency and mass changes, respectively, C_f the sensitivity factor for the crystal (C_f = 56.6 Hz μg^{-1} cm^2 for a 5 MHz AT-cut quartz crystal at room temperature), Q the charge passed and F the Faraday constant. M and z are the molar mass and charge of the ions/moieties.

Electrochemical Measurements: For cyclic voltammetry (CV) and chronoamperometry (potential step technique), the working electrode used was the QCM crystal in its E-QCM holder. For all measurements,

a PGSTAT302 potentiostat (Autolab, the Netherlands) and GPES control software were used with a standard 3-electrode cell. The counter electrode was a platinum plate (5 cm^2 per side) and a saturated mercury sulfate reference electrode (MSE) was used to avoid chloride contamination. All potentials reported in this article are quoted against the MSE. The glassware, as well as the QCM holder, was carefully cleaned with concentrated HCl and HNO_3 to remove any trace of protein. The electrolyte was prepared using MilliQ water (18.2 MΩ cm), then deaerated and protected whenever possible with paraffin film. Measurements were carried out with a flow of Ar above the electrolyte to avoid oxygen contamination. Typically 40 mL of electrolyte were used each time and all measurements recorded at room temperature. For each CV measurement, the potential was swept at a scan rate of 10 mV s^{-1} between –0.3 V and +0.3 V vs MSE for three cycles.

AFM Imaging: AFM samples were imaged using a Dimension 3100 (Digital Instruments - Veeco, NY, USA) equipped with a Nanoscope V controller supported by a vibration isolation bench (TMC, MA, USA). Silicon cantilevers (Olympus, Japan) were used (42 N m^{-1}, 300 kHz). The images were then processed with Image SXM v1.9 for background correction.

Supporting Information

Supporting Information is available from the Wiley Online Library or from the author.

Acknowledgements

The authors thank Prof. Ian Manners for initial discussions and the use of materials and laboratory equipment. This work was funded by the EPSRC (grant EP/F044437/1) and partly carried out under the European Union's Seventh Framework Programme (FP7/2007-2013) under Grant Agreement no. 228673 (MAGNONICS) and with the support of the Bristol Centre for Nanoscience and Quantum Information (NSQI).

Received: January 23, 2012
Revised: March 22, 2012
Published online: April 23, 2012

[1] a) G. M. Whitesides, E. Ostuni, S. Takayama, X. Jiang, D. E. Ingber, *Annu. Rev. Biomed. Eng.* **2001**, *3*, 335; b) T. G. Fernandes, M. M. Diogo, D. S. Clark, J. S. Dordick, J. M. S. Cabral, *Trends Biotechnol.* **2009**, *27*, 342.
[2] R. V. Martínez, J. Martínez, M. Chiesa, R. Garcia, E. Coronado, E. Pinilla-Cienfuegos, S. Tatay, *Adv. Mater.* **2010**, *22*, 588.
[3] S. S. Mark, M. Bergkvist, X. Yang, L. M. Teixeira, P. Bhatnagar, E. R. Angert, C. A. Batt, *Langmuir* **2006**, *22*, 3763.
[4] S. Kumagai, T. Ono, S. Yoshii, A. Kadotani, R. Tsukamoto, K. Nishio, M. Okuda, I. Yamashita, *Appl. Phys. Express* **2010**, *3*, 015101.
[5] a) K. L. Christman, V. D. Enriquez-Rios, H. D. Maynard, *Soft Matter* **2006**, *2*, 928; b) W. Wang, T. Gutu, D. K. Gale, J. Jiao, G. L. Rorrer, C.-H. Chang, *J. Am. Chem. Soc.* **2009**, *131*, 4178.
[6] a) S. Kumagai, S. Yoshii, K. Yamada, N. Matsukawa, I. Fujiwara, K. Iwahori, I. Yamashita, *Appl. Phys. Lett.* **2006**, *88*, 153103; b) S. R. Coyer, A. J. García, E. Delamarche, *Angew. Chem. Int. Ed.* **2007**, *46*, 6837.
[7] G. Singh, S. Pillai, A. Arpanaei, P. Kingshott, *Adv. Mater.* **2011**, *23*, 1519.
[8] H. Masuda, H. Hogi, K. Nishio, F. Matsumoto, *Chem. Lett.* **2004**, *33*, 812.
[9] Y. Hu, D. Chen, S. Park, T. Emrick, T. P. Russell, *Adv. Mater.* **2010**, *22*, 2583.
[10] a) K. H. A. Lau, J. Bang, D. H. Kim, W. Knoll, *Adv. Funct. Mater.* **2008**, *18*, 3148; b) N. Kumar, J. Hahm, *Langmuir* **2005**, *21*, 6652.
[11] M. A. Cole, N. H. Voelcker, H. Thissen, H. J. Griesser, *Biomaterials* **2009**, *30*, 1827.
[12] a) F. S. Bates, *Science* **1991**, *251*, 898; b) P. Alexandridis, B. Lindman, *Amphiphilic Block Copolymers: Self-Assembly and Applications*, Elsevier, Amsterdam **2000**.
[13] G. Krausch, R. Magerle, *Adv. Mater.* **2002**, *14*, 1579.
[14] a) I. Manners, *Chem. Commun.* **1999**, 857; b) G. R. Whittell, M. D. Hager, U. S. Schubert, I. Manners, *Nat. Mater.* **2011**, *10*, 176.
[15] R. Rulkens, A. J. Lough, I. Manners, S. R. Lovelace, C. Grant, W. E. Geiger, *J. Am. Chem. Soc.* **1996**, *118*, 12683.
[16] J.-C. Eloi, D. A. Rider, G. Cambridge, G. R. Whittell, M. A. Winnik, I. Manners, *J. Am. Chem. Soc.* **2011**, *133*, 8903.
[17] X. Wang, L. Wang, J. Wang, T. Chen, *J. Phys. Chem. B* **2004**, *108*, 5627.
[18] J. K. Li, S. Zou, D. A. Rider, I. Manners, G. C. Walker, *Adv. Mater.* **2008**, *20*, 1989.
[19] For examples of applications using the redox properties of PFS see: a) A. C. Arsenault, D. P. Puzzo, I. Manners, G. A. Ozin, *Nat. Photonics* **2007**, *1*, 468; b) Y. Ma, W.-F. Dong, M. A. Hempenius, H. Möhwald, G. J. Vancso, *Nat. Mater.* **2006**, *5*, 724.
[20] M. Uchida, M. T. Klem, M. Allen, P. Suci, M. Flenniken, E. Gillitzer, Z. Varpness, L. O. Liepold, M. Young, T. Douglas, *Adv. Mater.* **2007**, *19*, 1025.
[21] I. Yamashita, K. Iwahori, S. Kumagai, *Biochim. Biophys. Acta* **2010**, *1800*, 846.
[22] M. Okuda, K. Iwahori, I. Yamashita, H. Yoshimura, *Biotechnol. Bioeng.* **2003**, *84*, 187.
[23] B. Hennequin, L. Turyanska, T. Ben, A. M. Beltrán, S. I. Molina, M. Li, S. Mann, A. Patanè, N. R. Thomas, *Adv. Mater.* **2008**, *20*, 3592.
[24] T. Ueno, M. Suzuki, T. Goto, T. Matsumoto, K. Nagayama, Y. Watanabe, *Angew. Chem. Int. Ed.* **2004**, *43*, 2527.
[25] M. T. Klem, D. A. Resnick, K. Gilmore, M. Young, Y. U. Idzerda, T. Douglas, *J. Am. Chem. Soc.* **2007**, *129*, 197.
[26] M. Okuda, Y. Kobayashi, K. Suzuki, K. Sonoda, T. Kondoh, A. Wagawa, A. Kondo, H. Yoshimura, *Nano Lett.* **2005**, *5*, 991.
[27] X. Qu, N. Kobayashi, T. Komatsu, *ACS Nano* **2010**, *4*, 1732.
[28] a) R. D. Tilton, C. R. Robertson, A. P. Gast, *Langmuir* **1991**, *7*, 2710; b) Z. Zhang, Y. Lang, P. Liang, C. Li, S. Fang, *Polym. Int.* **2011**, *60*, 703; c) R. A. Hartvig, M. van de Weert, J. Østergaard, L. Jorgensen, H. Jensen, *Langmuir* **2011**, *27*, 2634.
[29] P. T. Varineau, D. A. Buttry, *J. Phys. Chem.* **1987**, *91*, 1292.
[30] D. A. Rider, K. A. Cavicchi, L. Vanderark, T. P. Russell, I. Manners, *Macromolecules* **2007**, *40*, 3790.
[31] Y. Li, J. Q. Pham, K. P. Johnston, P. F. Green, *Langmuir* **2007**, *23*, 9785.
[32] F. Caruso, D. N. Furlong, P. Kingshott, *J. Colloid Interface Sci.* **1997**, *186*, 129.
[33] a) M. Péter, M. A. Hempenius, E. S. Kooij, T. A. Jenkins, S. J. Roser, W. Knoll, G. J. Vancso, *Langmuir* **2004**, *20*, 891; b) S. Zou, M. A. Hempenius, H. Schönherr, G. J. Vancso, *Macromol. Rapid Commun.* **2006**, *27*, 103.
[34] S. Park, D. H. Lee, J. Xu, B. Kim, S. W. Hong, U. Jeong, T. Xu, T. P. Russell, *Science* **2009**, *323*, 1030.
[35] E. Palleau, N. M. Sangeetha, G. Viau, J.-D. Marty, L. Ressier, *ACS Nano* **2011**, *5*, 4228.
[36] V. V. Kruglyak, S. O. Demokritov, D. Grundler, *J. Phys. D* **2010**, *43*, 264001.
[37] D. A. Rider, K. A. Cavicchi, K. N. Power-Billard, T. P. Russell, I. Manners, *Macromolecules* **2005**, *38*, 6931.
[38] M. Peter, R. G. H. Lammertink, M. A. Hempenius, M. van Os, M. W. J. Beulen, D. N. Reinhoudt, W. Knoll, G. J. Vancso, *Chem. Commun.* **1999**, 359.
[39] M. Bradford, *Anal. Biochem.* **1976**, *72*, 248.
[40] K. A. Marx, *Biomacromolecules* **2003**, *4*, 1099.
[41] G. Sauerbrey, *Z. Phys.* **1959**, *155*, 206.